Title

HR-MAS MRS of the pancreas reveals reduced lipid and elevated lactate and taurine associated with early pancreatic cancer

Authors

Wang, Alan S
Lodi, Alessia
Rivera, Lee B
et al.

HR-MAS MRS of the pancreas reveals reduced lipid and elevated lactate and taurine associated with early pancreatic cancer

Alan S. Wang[a,†], **Alessia Lodi**[a,†], **Lee B. Rivera**[b], **Jose L. Izquierdo-Garcia**[a], **Matthew A. Firpo**[c], **Sean J. Mulvihill**[c], **Margaret A. Tempero**[d], **Gabriele Bergers**[b], and **Sabrina M. Ronen**[a,*]

[a]Department of Radiology and Biomedical Imaging, University of California San Francisco, San Francisco, CA, USA

[b]Department of Neurological Surgery, Helen Diller Family Comprehensive Cancer Center, University of California San Francisco, San Francisco, CA, USA

[c]Department of Surgery, Huntsman Cancer Institute, University of Utah, Salt Lake City, UT, USA

[d]Department of Medicine, Division of Hematology and Oncology, Helen Diller Family Comprehensive Cancer Center, University of California San Francisco, San Francisco, CA, USA

Abstract

The prognosis for patients with pancreatic cancer is extremely poor, as evidenced by the disease's five-year survival rate of ~5%. New approaches are therefore urgently needed to improve detection, treatment, and monitoring of pancreatic cancer. MRS-detectable metabolic changes provide useful biomarkers for tumor detection and response-monitoring in other cancers. The goal of this study was to identify MRS-detectable biomarkers of pancreatic cancer that could enhance currently available imaging approaches. We used ^{1}H high-resolution magic angle spinning MRS to probe metabolite levels in pancreatic tissue samples from mouse models and patients. In mice, the levels of lipids dropped significantly in pancreata with lipopolysaccharide-induced inflammation, in pancreata with pre-cancerous metaplasia (4 week old *p48-Cre;LSL-Kras^{G12D}* mice), and in pancreata with pancreatic intraepithelial neoplasia, which precedes invasive pancreatic cancer (8 week old *p48-Cre LSL-Kras^{G12D}* mice), to $26 \pm 19\%$ ($p = 0.03$), $19 \pm 16\%$ ($p = 0.04$), and $26 \pm 10\%$ ($p = 0.05$) of controls, respectively. Lactate and taurine remained unchanged in inflammation and in pre-cancerous metaplasia but increased significantly in pancreatic intraepithelial neoplasia to $266 \pm 61\%$ ($p = 0.0001$) and $999 \pm 174\%$ ($p < 0.00001$) of controls, respectively. Importantly, analysis of patient biopsies was consistent with the mouse findings. Lipids dropped in pancreatitis and in invasive cancer biopsies to $29 \pm 15\%$ ($p = 0.01$) and $26 \pm 38\%$ ($p = 0.02$) of normal tissue. In addition, lactate and taurine levels remained unchanged in inflammation but rose in tumor samples to $244 \pm 155\%$ ($p = 0.02$) and $188 \pm 67\%$ ($p = 0.02$), respectively, compared with normal tissue. Based on these findings, we propose that a drop in lipid levels could serve to inform on pancreatitis and cancer-associated inflammation, whereas elevated lactate and taurine could serve to identify the presence of pancreatic intraepithelial neoplasia and

*Correspondence to: Sabrina M. Ronen, Department of Radiology and Biomedical Imaging, University of California San Francisco, San Francisco, CA, USA. Sabrina.Ronen@ucsf.edu.

†These authors contributed equally to the work.

invasive tumor. Our findings may help enhance current imaging methods to improve early pancreatic cancer detection and monitoring.

Keywords

pancreatic cancer; PDAC; HR-MAS; lipid; lactate; taurine

INTRODUCTION

Pancreatic cancer is currently the fourth most common cause of cancer-related deaths in the United States (1,2). Patients with pancreatic ductal adenocarcinoma (PDAC), the most common type of pancreatic cancer, have a five-year survival rate as low as 5% (1,2). The prognosis for these patients is poor primarily because the disease is diagnosed late (1,2). Only 10–20% of patients present with a resectable disease. Of these patients, 80% will relapse after resection followed by adjuvant therapy. The remaining patients present with locally advanced unresectable disease or with detectable metastases. A family history of the disease dramatically increases the risk of developing PDAC by up to 50-fold (1,2). In addition, patients suffering from chronic pancreatitis have a higher incidence of PDAC, congruent with the observation that innate immune cells promote pancreatic intraepithelial neoplasia (PanIN), a precursor of PDAC, in pancreatic mouse tumor models (3,4). Indeed, PDAC is notable for its remarkable degree of desmoplasia, by which tumor cells are encased in a high-pressure, fibrous stromal mass composed of a dense extracellular matrix and various stromal cell types including large numbers of inflammatory cells (1,5,6). Unfortunately, current screening methods lack specificity to detect malignant transformation at an early stage or suffer from a high rate of false positives (7,8). There is thus a pressing need to develop additional biomarkers of pancreatic tumorigenesis that can enhance current imaging methods, particularly in high-risk patients, to improve early disease detection and to potentially serve to monitor response to therapy.

Previous studies have shown that MRS, a noninvasive and nondestructive imaging method, can help inform on oncogenic transformation, cancer progression, and response to therapy by effectively probing the levels of endogenous metabolites *in vivo* (9–14). Most notably, three-dimensional ^{1}H MRSI used in conjunction with a clinical MRI examination revealed significantly elevated levels of choline-containing metabolites (tCho) and decreased levels of citrate in prostatic adenocarcinomas in comparison to healthy prostatic tissue (15,16). MRSI of the breast also detected elevated tCho levels in cancerous tissue (17–19), while MRSI of the brain revealed an elevated tCho to *N*-acetylaspartate ratio in brain tumors when compared with normal tissue (20–22).

In the case of pancreatic cancer, the 90% prevalence of mutant *Kras* is likely to lead to MRS-detectable differences in PDAC metabolism when compared with normal tissue (1,5). Indeed, mutant *Kras* has well-established roles in tumor growth, angiogenesis, and metastasis, but recent findings indicate that mutant *Kras* also plays a pivotal role in reprogramming a variety of metabolic pathways (23–26). Specifically, mutant *Kras* induces pancreatic cancer cells to increase their glucose uptake, glycolytic flux, and lactate

production by regulating the transcription of a variety of genes (26). The mutation also directs glucose metabolites towards anabolic hexosamine biosynthesis and the non-oxidative pentose phosphate pathway (26). Mutant *Kras* also plays a notable role in promoting ribose biogenesis and altering glutamine metabolism (25,26). To date, only a few clinical studies have been published that attempted to use *in vivo* ^{1}H MRS to monitor pancreatic cancer, and the authors found that pancreatic cancer was associated with lowered lipid levels (27,28). In addition, previous studies have used ^{1}H high-resolution magic angle spinning (HR-MAS) MRS to detect elevated levels of lactate in swine with moderate to severe pancreatitis and elevated levels of lactate and taurine in both rats with pancreatic cancer and a mouse xenograft model of pancreatic cancer (29–31).

In this context, the goal of this study was to use ^{1}H HR-MAS MRS to examine both mouse and patient pancreatic tissue samples and compare the metabolic profiles of normal, inflamed (pancreatitis), early PanIN, and invasive PDAC tissue. We show that high lipid levels present in a healthy pancreas drop significantly in the presence of inflammation, pre-cancerous metaplasia, pre-invasive PanIN lesions, and invasive PDAC. We also show that lactate and taurine levels are elevated in PanIN and in PDAC but not in inflammation. Our findings may aid in the development of novel imaging approaches for early detection of pancreatic cancer.

EXPERIMENTAL DETAILS

Mouse pancreatic samples

All mice (*Mus musculus*) used in the study were mice that had been maintained in the inbred C57BL/6 genetic background by continuously breeding with the pure C57BL/6 mouse strain. As a model for early pancreatic cancer development we used *p48-Cre;LSL-Kras^{G12D}* mice (hereafter referred to as *Kras* mice), which are known to develop PanIN lesions over time. The mice were generated by crossing mice expressing either *p48-Cre* or *LSL-Kras^{G12D}* as previously described (3). *Kras* mice were sacrificed, and pancreatic tissue samples were collected at 4 weeks ($n = 6$) and 8 weeks ($n = 6$) for further analysis. All samples were divided in two to provide tissue specimens for both histological and HR-MAS analysis. Samples for HR-MAS analysis were immediately snap frozen in liquid nitrogen and stored at −80 °C. Samples for histology were placed in paraformaldehyde.

Samples with pancreatic inflammation ($n = 8$) were obtained from 6–8 week old mice treated with lipopolysaccharide (LPS, Sigma) via intraperitoneal injection (32). These mice were either treated with 2 mg/kg LPS for five consecutive days and sacrificed three hours after the last dose or treated with 10 mg/kg LPS once and sacrificed twelve hours later. Importantly, the two treatment groups were indistinguishable by histology (see below) and thus all LPS data were grouped together. Control pancreatic tissue samples ($n = 9$) were obtained from 6–8 week old mice treated with phosphate buffered saline (PBS). These mice were sacrificed and pancreatic tissue samples from all mice were collected for further histological and HR-MAS analysis as above.

Histology of mouse pancreatic samples

Pancreatic samples from PBS-treated, LPS-treated, and *Kras* mice were fixed in 1% paraformaldehyde at 4 °C for 1 hour immediately after excision. Samples were washed in ice-cold PBS, incubated in 30% sucrose, and then embedded in OCT compound (Tissue Tek). Frozen sections were prepared using a Cryostat (Leica). For hematoxylin and eosin staining, sections were treated with 1% paraformaldehyde for 30 minutes, washed, and then stained. Sections were then dehydrated and mounted in a xylene-based mounting medium. For antibody staining, tissue was incubated with 1% paraformaldehyde for 5 minutes. Fixed sections were washed in wash buffer, blocked, and then incubated with phycoerythrin-conjugated rat anti-mouse CD11b (BioLegend). Stained sections were washed and mounted in Prolong with DAPI (Molecular Probes). All images were visualized and captured using a Zeiss Observer Z1 microscope with AxioVision software (Zeiss).

Patient pancreatic samples

Patient-matched cancerous and uninvolved needle core biopsies ($n = 7$) were obtained during or immediately following surgical resection of the pancreas at the University of Utah School of Medicine. Six of the paired samples were obtained from a Whipple procedure, and one pair was taken through a distal pancreatectomy. Cancerous biopsies were obtained from the palpated tumor while uninvolved biopsies were obtained from regions of the pancreas distal to the tumor. In addition, pancreatitis samples ($n = 5$) and two patient-matched pancreatitis and grossly uninvolved tissue samples ($n = 2$) were also obtained from the University of Utah School of Medicine. All samples were snap frozen in cryogenic vials and stored at −80 °C until HR-MAS analysis. The pathology of all tissue samples was confirmed histologically by inspection of an adjacent tissue sample by an experienced pathologist.

¹H HR-MAS NMR spectroscopy

All samples were weighed (4.1–37.6 mg) and inserted into zirconia rotors along with 6 μl of deuterium oxide with 0.75 weight percent 2,2,3,3-D4-3-(trimethylsilyl)propionic acid, which was used as a chemical shift reference. Samples were spun at 2250 rpm on a Varian (Agilent) Inova 500 MHz spectrometer and maintained at 1 °C throughout the acquisition time. Spectra were acquired using a pulse–acquire sequence with a 90° pulse, a 20 kHz spectral width, a 2 s acquisition time, a 2 s water presaturation delay, 128 transients, and four steady state pulses. In addition, to minimize the broad signal contributions from lipids and macromolecules, a Carr–Purcell–Meiboom–Gill (CPMG) sequence was used with a 144 ms echo time (train of 162 180° hard pulses 0.888 μs apart) and 512 transients. Data acquisition was kept to a minimum (between 60 and 90 min). Spectra were analyzed using MestReNova (Santiago de Compostela, Spain). All spectra were first normalized to the electronic reference to access *in vivo* concentrations before metabolite peaks were deconvoluted and peak integrals were measured. The peak integrals were then normalized to the sample mass.

Statistics

All data are reported as the mean ± standard deviation. Statistical significance was determined using the Student *t*-test (paired *t*-test when considering patient-matched samples

and unpaired t-test in all other cases). A p-value less than or equal to 0.05 was considered significant.

RESULTS

Mouse models

To determine the metabolic sequelae of early events associated with tumor development, we wanted to investigate inflamed pancreata and pancreata with early PanIN lesions. To this end, we used mice treated with LPS, which is known to induce inflammation, and *Kras* mice, which are genetically engineered to develop PanIN lesions (3,32). Figure 1 illustrates the histology of our mouse models. In contrast to normal pancreata (Fig. 1(A)), pancreata from LPS-treated mice (Fig. 1(B)) were inflamed, as evidenced by the presence of inflammatory cells around the normal tissue and within the tissue vasculature. The pancreata of 4 week old *Kras* mice had evidence of a reactive stroma, infiltrating inflammatory cells, and acinar to ductal metaplasia. However, no evidence of PanIN or PDAC could be observed in those samples (Fig. 1(C)). As expected from this mouse model (3), the 8 week old *Kras* mice were further along in oncogenic progression and displayed a loss of acinar tissue, desmoplasia, and multiple PanIN lesions (Fig. 1(D)). However, no advanced PDAC tumors were detected in the 8 week old *Kras* mice either. In addition, we noted that none of the mice used in the study showed any weight loss.

To more specifically assess inflammation, we next examined CD11b + immune cell content. Immunofluorescent staining of tissue sections revealed that LPS treatment induced substantial infiltration of CD11b + cells (Fig. 2(A), (B)), thus confirming the presence of pancreatitis. A similar level of inflammation was also observed in both 4 week (Fig. 2(C)) and 8 week old (Fig. 2(D)) *Kras* mice, confirming that significant levels of inflammation are associated with early metaplasia and premalignant PanIN in our model.

Neoplasia is associated with low lipid and high lactate and taurine levels in mouse tissue samples

In order to compare the metabolic profiles of healthy and injured pancreata, we investigated 29 mouse pancreatic samples using HR-MAS ^{1}H NMR spectroscopy. Three typical pulse–acquire spectra, one from a wild type mouse treated with PBS, one from a wild type mouse treated with LPS, and one from a 4 week old *Kras* mouse, are shown in Fig. 3(A). They illustrate the presence of readily visible fatty acid signals at 0.91 (–CH_3), 1.30 (–(CH_2–)$_n$), 1.59 (–CH_2CH$_2$COO–), 2.05 (–CH_2CHCHCH$_2$–), 2.26 (–CH_2COO–), 2.89 (–CHCH_2CH–), and 5.34 (–CHCH–) ppm as well as two additional signals from the glycerol backbone of phospholipids at 4.09 and 4.30 ppm. They also illustrate a clear drop in all lipid signals when comparing tissue from *Kras* mice with tissue from PBS-treated wild type mice. Similar findings were observed when comparing LPS-induced pancreatic inflammation with normal pancreatic tissue. On average, the levels of lipids at 1.30 ppm dropped to $26 \pm 19\%$ ($p = 0.03$) for LPS-treated mice, $19 \pm 16\%$ ($p = 0.04$) for 4 week old *Kras* mice, and $26 \pm 10\%$ ($p = 0.05$) for 8 week old *Kras* mice when compared with controls (Fig. 3(B)). Because the lipid peak at 1.30 ppm overlaps with the lactate signal, similar analyses were performed with the lipid resonance at 1.59 ppm. The findings were comparable, with lipid

levels at 1.59 ppm dropping to $22 \pm 24\%$ ($p = 0.04$) for LPS-treated mice, $14 \pm 14\%$ ($p = 0.05$) for 4 week old *Kras* mice, and $14 \pm 12\%$ ($p = 0.05$) for 8 week old *Kras* mice when compared with controls.

Representative CPMG spectra of pancreata from wild type mice treated with PBS, wild type mice treated with LPS, and 8 week old *Kras* mice are shown in Fig. 4(A). Because the CPMG sequence suppresses the lipid peaks, we were able to monitor metabolites such as lactate, taurine, and tCho that are present at lower concentrations or overlap with lipids. On average, we did not detect a significant difference in any of these metabolites in pancreata with LPS-induced inflammation or in pancreata from 4 week old *Kras* mice when compared with controls. However, we observed a significant increase in both lactate and taurine levels in the pancreatic tissue samples of 8 week old *Kras* mice. Specifically, the lactate levels in the 8 week old *Kras* mice rose to $266 \pm 61\%$ ($p = 0.0001$) of controls while the taurine levels in these mice increased to $999 \pm 174\%$ ($p < 0.00001$) of controls. In addition, tCho was significantly lower in the pancreata of 8 week old *Kras* mice, dropping to $41 \pm 13\%$ ($p = 0.01$) of controls (Fig. 4(B)). This decrease was primarily due to a drop in phosphocholine levels to $24 \pm 18\%$ ($p = 0.02$) of controls.

PDAC is associated with low lipid and high lactate and taurine levels in human tissue samples

To determine whether our results from mouse pancreatic samples were relevant to human disease, we also examined patient samples from cases of pancreatitis and cases of resectable invasive PDAC. Three typical pulse–acquire spectra, one from an uninvolved biopsy, one from an inflamed pancreas, and one from a cancerous pancreas, are shown in Fig. 5(A). The spectra have similar features to those in the mouse pancreata, including prominent lipid peaks detectable in normal pancreata that clearly drop in the pancreatitis and tumor samples. To analyze the data, we considered that all our PDAC biopsies ($n = 7$) but only a subset ($n = 2$) of our pancreatitis biopsies ($n = 7$) had patient-matched uninvolved tissue samples. We therefore analyzed the clinical data in two different ways. We first compared all uninvolved biopsy samples with all pancreatitis samples and all PDAC samples without regard to patient matching. Similar to our results in mice, the levels of lipids at 1.30 ppm dropped to $29 \pm 15\%$ ($p = 0.01$) for the pancreatitis samples and to $26 \pm 38\%$ ($p = 0.02$) for the PDAC samples when compared with healthy pancreatic samples (Fig. 5(B)). We then compared the PDAC samples with their matched uninvolved biopsy samples and the two pancreatitis samples with their matched uninvolved biopsy samples. Importantly, this analysis yielded very similar results. In the PDAC biopsies, the levels of lipids at 1.30 ppm dropped significantly to $28 \pm 29\%$ ($p = 0.03$) of the levels in uninvolved biopsies (Fig. 5(C)). In pancreatitis samples, the lipids at 1.30 ppm dropped to $30 \pm 13\%$ ($n = 2$) when compared with uninvolved biopsies.

Typical patient CPMG spectra are shown in Fig. 6(A) and also illustrate features similar to those observed in mice, most notably an increase in lactate and taurine associated with PDAC. Specifi-cally, in the global analysis of all patient samples, lactate levels rose significantly in PDAC to $244 \pm 155\%$ ($p = 0.02$) of healthy tissue while taurine levels increased significantly to $188 \pm 67\%$ ($p = 0.02$) of healthy tissue (Fig. 6(B)). Similarly, when

considering patient-matched data, we observed a significant increase in lactate to 271 $\pm$ 130% ($p = 0.03$) of matched controls while taurine levels rose significantly to 291 $\pm$ 171% ($p = 0.01$) of matched controls. No significant differences in tCho were detected in either analysis. In pancreatitis samples, lactate, taurine, and tCho levels remained, within experimental error, unchanged.

DISCUSSION

There is a pressing need to improve the stark prognosis of PDAC patients (1,2). In an effort to address this need, we sought to determine if there are any MRS-detectable metabolic changes associated with pancreatic cancer onset that could serve to enhance currently available imaging approaches and thus improve early detection and monitoring of the disease. To this end, we first investigated mouse pancreata and then confirmed the clinical significance of our findings by investigating patient biopsies.

We used the previously described *Kras* (*p48-Cre;LSL-Kras*[G12D]) mice (3) and LPS-treated mice (32) as model systems. Importantly, as previously described, the *Kras* model develops early pre-neoplastic PanIN lesions but only rarely develops late PDAC tumors. This provided us with a unique approach to probe the metabolic alterations associated with the early stages of tumor development. With regard to our pancreatitis model, LPS treatment leads to systemic inflammation and is therefore not a perfect approach to model inflammation of the pancreas. Nonetheless, because our studies histologically confirmed the presence of inflammation in the pancreas, we felt that this approach was valid. Importantly, our findings in LPS-treated mice were consistent with observations in patients with pancreatitis.

In healthy pancreatic samples we found strikingly high levels of MRS-detectable mobile fatty acids. The standard deviation in lipid content for the normal mouse and human samples is somewhat high, possibly due to variation in the amount of pancreatic fat healthy pancreata develop, which can vary widely (33). Nonetheless, lipid levels dropped significantly in mouse pancreata with LPS-induced inflammation and in pancreata from *Kras* mice with precancerous metaplasia or early PanIN lesions. They also dropped in samples from patients with pancreatitis and in samples from patients with resectable PDAC.

With regard to the drop in lipid levels, any direct quantitative comparison with other types of cancer is challenging. Some previous HR-MAS studies do not report on lipids, while others report that lipid levels remain high (e.g. breast cancer) or drop (e.g. co-lorectal cancer) (34–36). Furthermore, previous studies have detected an increase rather than a drop in fatty acid synthesis in most cancer types (37). Elevated lipid levels have been detected by MRS in several cancers, and elevated lipids are associated with necrotic regions in advanced tumors (37–42). Nonetheless, our observations are consistent with previous studies using *in vivo* ^{1}H MRS in pancreatic cancer patients that reported significantly lower lipid levels in tumor when compared with normal pancreatic tissue (27,28). Our findings are also in line with a previous mass spectrometry study of PDAC in rats that found that tumorigenesis was associated with a decrease in the levels of many fatty acids (43). When comparing PDAC and pancreatitis, our study did not detect a significant difference in lipid levels between

these samples. Our results thus stand in contrast to another study that used *in vivo* ^{1}H MRS in patients and found that lipid levels were lower in patients with pancreatitis than those with PDAC (44). However, the authors of that study acknowledge that their findings could be complicated by peripancreatic tissue contaminating the area examined.

When considering our mouse histological data, the drop in lipids could be associated with the presence of infiltrating in-flammatory cells, which were absent from normal pancreata but which were clearly detectable in pancreata from LPS-treated mice, 4 week old *Kras* mice, and 8 week old *Kras* mice. Further studies are required to confirm a link between the drop in lipids and inflammation, but one possible mediator could be pancreatic stellate cells (PSCs). In a healthy pancreas, PSCs help maintain the normal architecture of the pancreas (45–47). Importantly, these PSCs contain elevated levels of cytoplasmic vitamin A-containing lipid droplets. Inflammation and early tumorigenesis are associated with PSC activation and differentiation to a myofibroblast phenotype associated with deposition of extracellular matrix proteins, which, in turn, can facilitate cancer progression. PSC activation and differentiation are also associated with loss of cytoplasmic lipid droplets (45–47) and thus could explain the changes in lipid levels observed in inflammation and early tumor development in our studies. However, PSCs comprise only about 5% of the pancreatic volume and may not be the only explanation for the drop in lipid levels observed in our samples (45). Indeed, previous reports indicate that the median intra-pancreatic fat composition in a normal pancreas is around 10% (33). The replacement of this fat by cancerous or infiltrating immune cells could decrease the MRS-detectable lipid content. In addition, we cannot rule out the possibility that pancreatic lipases, which may become active within the pancreas during inflammation, are responsible for the drop in lipid levels.

Importantly, our studies revealed that lactate and taurine levels increased significantly in 8 week old *Kras* mice but remained unchanged in 4 week old *Kras* mice and in mice with LPS-induced inflammation. Similarly, lactate and taurine levels were comparable to those in healthy tissue in patient pancreatitis, but increased significantly in PDAC. Histologically, only 8 week old *Kras* mice pancreata showed the presence of PanIN, indicating that elevated lactate and taurine are likely associated with early tumor development and could thus serve as potential early biomarkers of pancreatic cancer.

The increase in lactate levels observed in our PanIN and PDAC samples is consistent with previous work demonstrating that mutant *Kras* induces pancreatic cancer cells to increase their glucose uptake, glycolytic flux, and lactate production (26). This preference of cancer cells to rely on aerobic glycolysis rather than oxidative phosphorylation to generate necessary energy (also termed the Warburg effect) has been well documented in many types of cancer (48). It is currently hypothesized that this enhancement of aerobic glycolysis supports various biosynthetic pathways to satisfy the metabolic requirements of proliferation (48). Previous HR-MAS studies have found evidence for the War-burg effect in various pancreatitis and pancreatic cancer animal models (29–31). Elevated lactate levels have also been detected in the serum of patients (49).

The increase in lactate levels may also be attributed to increased hypoxia in pancreatic cancers and their inability to remove lactate from the tumor microenvironment. Recent

studies have found that pancreatic cancers have abnormally high levels of stroma and inflammation and relatively low levels of vasculature (50,51). The dense stroma distorts the normal architecture of the tissue and limits the diffusion of oxygen by tightening the capillary network (46). In addition, the high levels of desmoplasia generate elevated levels of interstitial fluid pressures, causing the vasculature to collapse and impeding traffic of small molecules around the tumor (51). As the vasculature becomes more and more distorted, it may become increasingly difficult for lactate produced by the tumor to escape its microenvironment.

Taurine is an organic acid implicated in several physiological functions. Our findings that taurine levels are elevated in PanIN and PDAC are consistent with previous studies of pancreatic cancer (29,30,52). Elevated taurine levels have also been reported in other cancer types (35,52–55). The increase in taurine could be a result of an influx of immune cells, which have high levels of this organic acid (56,57). Taurine has roles in fat absorption and oxidation, and some studies suggest that taurine is associated with apoptosis (52,58,59). However, the specific role of taurine in cancer has yet to be fully understood.

In our study tCho levels dropped in mouse pancreata with PanIN and remained unchanged in patient PDAC samples. These findings are in contrast to recent work in human pancreatic cell lines that found an increase in tCho and phosphocholine when comparing PDAC cells with immortalized pancreatic cells (60). The same study also found an increase in the expression of choline kinase, which catalyzes the synthesis of phosphocholine. Elevated phosphocholine and tCho levels as well as overexpression of choline kinase are typically associated with malignant transformation in almost every cancer type examined (15–22,61). Our findings are therefore surprising. One possible explanation, particularly in patients, could be that the aforementioned poor vascularization of pancreatic tumors is limiting the delivery of choline to the tumor site. Further studies are needed to clarify this point.

In summary, we have identified potential metabolic biomarkers of pancreatitis and tumor-associated inflammation as well as metabolic biomarkers of PanIN and early stage PDAC. Our results suggest that the drop in lipid levels may be associated with inflammation during early tumor development, whereas the increase in lactate and taurine levels may be associated with tumor onset and progression. Further methodological developments are required to translate these biomarkers to the clinical setting, likely requiring rapid high-resolution metabolic imaging approaches. Nonetheless, combining such metabolic imaging with currently available methods could help enhance the early detection, characterization, and response-monitoring of PDAC patients. Furthermore, it could aid in screening of high-risk patients. Ultimately, by helping detect the presence of tumor at an early time point prior to widespread metastasis and at a point when resection is possible, our findings could help improve the prognosis of PDAC patients.

Acknowledgments

Abbreviations

PDAC	pancreatic ductal adenocarcinoma
PanIN	pancreatic intraepithelial neoplasia
tCho	total choline
HR-MAS	high-resolution magic angle spinning
LPS	lipopolysaccharide
PBS	phosphate buffered saline
CPMG	Carr–Purcell–Meiboom–Gill
PSC	pancreatic stellate cell

References

1. Hidalgo M. Pancreatic cancer. N Engl J Med. 2010; 362(17):1605–1617. [PubMed: 20427809]

2. American Cancer Society. Cancer Facts and Figures. American Cancer Society; Atlanta, GA: 2014.

3. Hingorani SR, Petricoin EF, Maitra A, Rajapakse V, King C, Jacobetz MA, Ross S, Conrads TP, Veenstra TD, Hitt BA, Kawaguchi Y, Johann D, Liotta LA, Crawford HC, Putt ME, Jacks T, Wright CV, Hruban RH, Lowy AM, Tuveson DA. Preinvasive and invasive ductal pancreatic cancer and its early detection in the mouse. Cancer Cell. 2003; 4(6):437–450. [PubMed: 14706336]

4. Raimondi S, Maisonneuve P, Lowenfels AB. Epidemiology of pancreatic cancer: an overview. Nat Rev Gastroenterol Hepatol. 2009; 6(12):699–708. [PubMed: 19806144]

5. Bardeesy N, DePinho RA. Pancreatic cancer biology and genetics. Nat Rev Cancer. 2002; 2(12): 897–909. [PubMed: 12459728]

6. Chu GC, Kimmelman AC, Hezel AF, DePinho RA. Stromal biology of pancreatic cancer. J Cell Biochem. 2007; 101(4):887–907. [PubMed: 17266048]

7. Muniraj T, Jamidar PA, Aslanian HR. Pancreatic cancer: a comprehensive review and update. Dis Mon. 2013; 59(11):368–402. [PubMed: 24183261]

8. Vincent A, Herman J, Schulick R, Hruban RH, Goggins M. Pancreatic cancer. Lancet. 2011; 378(9791):607–620. [PubMed: 21620466]

9. Al-Saffar NM, Titley JC, Robertson D, Clarke PA, Jackson LE, Leach MO, Ronen SM. Apoptosis is associated with triacylglycerol accumulation in Jurkat T-cells. Br J Cancer. 2002; 86(6):963–970. [PubMed: 11953830]

10. Bolan PJ, Nelson MT, Yee D, Garwood M. Imaging in breast cancer: magnetic resonance spectroscopy. Breast Cancer Res. 2005; 7(4):149–152. [PubMed: 15987466]

11. Evelhoch JL, Gillies RJ, Karczmar GS, Koutcher JA, Maxwell RJ, Nalcioglu O, Raghunand N, Ronen SM, Ross BD, Swartz HM. Applications of magnetic resonance in model systems: cancer therapeutics. Neoplasia. 2000; 2(1/2):152–165. [PubMed: 10933074]

12. Lodi A, Ronen SM. Magnetic resonance spectroscopy detectable metabolomic fingerprint of response to antineoplastic treatment. PLoS One. 2011; 6(10):e26155. [PubMed: 22022547]

13. McKnight TR. Proton magnetic resonance spectroscopic evaluation of brain tumor metabolism. Semin Oncol. 2004; 31(5):605–617. [PubMed: 15497114]

14. Ross J, Najjar AM, Sankaranarayanapillai M, Tong WP, Kaluarachchi K, Ronen SM. Fatty acid synthase inhibition results in a magnetic resonance-detectable drop in phosphocholine. Mol Cancer Ther. 2008; 7(8):2556–2565. [PubMed: 18723500]

15. Kurhanewicz J, Vigneron DB, Hricak H, Narayan P, Carroll P, Nelson SJ. Three-dimensional H-1 MR spectroscopic imaging of the in situ human prostate with high (0.24–0.7–cm^3) spatial resolution. Radiology. 1996; 198(3):795–805. [PubMed: 8628874]

16. Scheidler J, Hricak H, Vigneron DB, Yu KK, Sokolov DL, Huang LR, Zaloudek CJ, Nelson SJ, Carroll PR, Kurhanewicz J. Prostate cancer: localization with three-dimensional proton MR spectroscopic imaging – clinicopathologic study. Radiology. 1999; 213(2):473–480. [PubMed: 10551229]

17. Gribbestad IS, Singstad TE, Nilsen G, Fjosne HE, Engan T, Haugen OA, Rinck PA. In vivo 1H MRS of normal breast and breast tumors using a dedicated double breast coil. J Magn Reson Imaging. 1998; 8(6):1191–1197. [PubMed: 9848727]

18. Kim JK, Park SH, Lee HM, Lee YH, Sung NK, Chung DS, Kim OD. In vivo 1H-MRS evaluation of malignant and benign breast diseases. Breast. 2003; 12(3):179–182. [PubMed: 14659324]

19. Kvistad KA, Bakken IJ, Gribbestad IS, Ehrnholm B, Lundgren S, Fjosne HE, Haraldseth O. Characterization of neoplastic and normal human breast tissues with in vivo ^{1}H MR spectroscopy. J Magn Reson Imaging. 1999; 10(2):159–164. [PubMed: 10441019]

20. Dowling C, Bollen AW, Noworolski SM, McDermott MW, Barbaro NM, Day MR, Henry RG, Chang SM, Dillon WP, Nelson SJ, Vigneron DB. Preoperative proton MR spectroscopic imaging of brain tumors: correlation with histopathologic analysis of resection specimens. Am J Neuroradiol. 2001; 22(4):604–612. [PubMed: 11290466]

21. Kurhanewicz J, Vigneron DB, Nelson SJ. Three-dimensional magnetic resonance spectroscopic imaging of brain and prostate cancer. Neoplasia. 2000; 2(1/2):166–189. [PubMed: 10933075]

22. Nelson SJ. Analysis of volume MRI and MR spectroscopic imaging data for the evaluation of patients with brain tumors. Magn Reson Med. 2001; 46(2):228–239. [PubMed: 11477625]

23. Collins MA, Pasca di Magliano M. Kras as a key oncogene and therapeutic target in pancreatic cancer. Front Physiol. 2013; 4:407. [PubMed: 24478710]

24. Morris JP, Wang SC, Hebrok M. KRAS, Hedgehog, Wnt and the twisted developmental biology of pancreatic ductal adenocarcinoma. Nat Rev Cancer. 2010; 10(10):683–695. [PubMed: 20814421]

25. Son J, Lyssiotis CA, Ying H, Wang X, Hua S, Ligorio M, Perera RM, Ferrone CR, Mullarky E, Shyh-Chang N, Kang Y, Fleming JB, Bardeesy N, Asara JM, Haigis MC, DePinho RA, Cantley LC, Kimmelman AC. Glutamine supports pancreatic cancer growth through a KRAS-regulated metabolic pathway. Nature. 2013; 496(7443):101–105. [PubMed: 23535601]

26. Ying H, Kimmelman AC, Lyssiotis CA, Hua S, Chu GC, Fletcher-Sananikone E, Locasale JW, Son J, Zhang H, Coloff JL, Yan H, Wang W, Chen S, Viale A, Zheng H, Paik JH, Lim C, Guimaraes AR, Martin ES, Chang J, Hezel AF, Perry SR, Hu J, Gan B, Xiao Y, Asara JM, Weissleder R, Wang YA, Chin L, Cantley LC, DePinho RA. Oncogenic Kras maintains pancreatic tumors through regulation of anabolic glucose metabolism. Cell. 2012; 149(3):656–670. [PubMed: 22541435]

27. Ma X, Zhao X, Ouyang H, Sun F, Zhang H, Zhou C, Shen H. The metabolic features of normal pancreas and pancreatic adenocarcinoma: preliminary result of in vivo proton magnetic resonance spectroscopy at 3.0 T. J Comput Assist Tomogr. 2011; 35(5):539–543. [PubMed: 21926845]

28. Yao X, Zeng M, Wang H, Fei S, Rao S, Ji Y. Metabolite detection of pancreatic carcinoma by in vivo proton MR spectroscopy at 3 T: initial results. Radiol Med. 2012; 117(5):780–788. [PubMed: 22095426]

29. Fang F, He X, Deng H, Chen Q, Lu J, Spraul M, Yu Y. Discrimination of metabolic profiles of pancreatic cancer from chronic pancreatitis by high-resolution magic angle spinning 1H nuclear magnetic resonance and principal components analysis. Cancer Sci. 2007; 98(11):1678–1682. [PubMed: 17727683]

30. He XH, Li WT, Gu YJ, Yang BF, Deng HW, Yu YH, Peng WJ. Metabonomic studies of pancreatic cancer response to radiotherapy in a mouse xenograft model using magnetic resonance spectroscopy and principal components analysis. World J Gastroenterol. 2013; 19(26):4200–4208. [PubMed: 23864784]

31. Sun G, Wang J, Zhang J, Ma C, Shao C, Hao J, Zheng J, Feng X, Zuo C. High-resolution magic angle spinning ^{1}H magnetic resonance spectroscopy detects choline as a biomarker in a swine obstructive chronic pancreatitis model at an early stage. Mol Biosyst. 2014; 10(3):467–474. [PubMed: 24342968]

32. Ding SP, Li JC, Jin C. A mouse model of severe acute pancreatitis induced with caerulein and lipopolysaccharide. World J Gastroenterol. 2003; 9(3):584–589. [PubMed: 12632523]

33. Tushuizen ME, Bunck MC, Pouwels PJ, Bontemps S, van Waesberghe JH, Schindhelm RK, Mari A, Heine RJ, Diamant M. Pancreatic fat content and beta-cell function in men with and without type 2 diabetes. Diabetes Care. 2007; 30(11):2916–2921. [PubMed: 17666465]

34. Li M, Song Y, Cho N, Chang JM, Koo HR, Yi A, Kim H, Park S, Moon WK. An HR-MAS MR metabolomics study on breast tissues obtained with core needle biopsy. PLoS One. 2011; 6(10):e25563. [PubMed: 22028780]

35. Mirnezami R, Jimenez B, Li JV, Kinross JM, Veselkov K, Goldin RD, Holmes E, Nicholson JK, Darzi A. Rapid diagnosis and staging of colorectal cancer via high-resolution magic angle spinning nuclear magnetic resonance (HR-MAS NMR) spectroscopy of intact tissue biopsies. Ann Surg. 2014; 259(6):1138–1149. [PubMed: 23860197]

36. Tessem MB, Swanson MG, Keshari KR, Albers MJ, Joun D, Tabatabai ZL, Simko JP, Shinohara K, Nelson SJ, Vigneron DB, Gribbestad IS, Kurhanewicz J. Evaluation of lactate and alanine as metabolic biomarkers of prostate cancer using ^{1}H HR-MAS spectroscopy of biopsy tissues. Magn Reson Med. 2008; 60(3):510–516. [PubMed: 18727052]

37. Menendez JA, Lupu R. Fatty acid synthase and the lipogenic phenotype in cancer pathogenesis. Nat Rev Cancer. 2007; 7(10):763–777. [PubMed: 17882277]

38. Delikatny EJ, Chawla S, Leung DJ, Poptani H. MR-visible lipids and the tumor microenvironment. NMR Biomed. 2011; 24(6):592–611. [PubMed: 21538631]

39. Zietkowski D, Davidson RL, Eykyn TR, De Silva SS, Desouza NM, Payne GS. Detection of cancer in cervical tissue biopsies using mobile lipid resonances measured with diffusion-weighted ^{1}H magnetic resonance spectroscopy. NMR Biomed. 2010; 23(4):382–390. [PubMed: 20014336]

40. Howe FA, Barton SJ, Cudlip SA, Stubbs M, Saunders DE, Murphy M, Wilkins P, Opstad KS, Doyle VL, McLean MA, Bell BA, Griffiths JR. Metabolic profiles of human brain tumors using quantitative in vivo ^{1}H magnetic resonance spectroscopy. Magn Reson Med. 2003; 49(2):223–232. [PubMed: 12541241]

41. Righi V, Mucci A, Schenetti L, Tosi MR, Grigioni WF, Corti B, Bertaccini A, Franceschelli A, Sanguedolce F, Schiavina R, Martorana G, Tugnoli V. Ex vivo HR-MAS magnetic resonance spectroscopy of normal and malignant human renal tissues. Anticancer Res. 2007; 27(5A):3195–3204. [PubMed: 17970061]

42. Calabrese C, Pisi A, Di Febo G, Liguori G, Filippini G, Cervellera M, Righi V, Lucchi P, Mucci A, Schenetti L, Tonini V, Tosi MR, Tugnoli V. Biochemical alterations from normal mucosa to gastric cancer by *ex vivo* magnetic resonance spectroscopy. Cancer Epidemiol Biomark Prev. 2008; 17(6):1386–1395.

43. Yabushita S, Fukamachi K, Tanaka H, Fukuda T, Sumida K, Deguchi Y, Mikata K, Nishioka K, Kawamura S, Uwagawa S. Metabolomic and transcriptomic profiling of human K-ras oncogene transgenic rats with pancreatic ductal adenocarcinomas. Carcinogenesis. 2013; 34(6):1251–1259. [PubMed: 23393225]

44. Cho SG, Lee DH, Lee KY, Ji H, Lee KH, Ros PR, Suh CH. Differentiation of chronic focal pancreatitis from pancreatic carcinoma by in vivo proton magnetic resonance spectroscopy. J Comput Assist Tomogr. 2005; 29(2):163–169. [PubMed: 15772531]

45. Apte MV, Wilson JS, Lugea A, Pandol SJ. A starring role for stellate cells in the pancreatic cancer microenvironment. Gastroenterology. 2013; 144(6):1210–1219. [PubMed: 23622130]

46. Erkan M, Hausmann S, Michalski CW, Fingerle AA, Dobritz M, Kleeff J, Friess H. The role of stroma in pancreatic cancer: diagnostic and therapeutic implications. Nat Rev Gastroenterol Hepatol. 2012; 9(8):454–467. [PubMed: 22710569]

47. Omary MB, Lugea A, Lowe AW, Pandol SJ. The pancreatic stellate cell: a star on the rise in pancreatic diseases. J Clin Invest. 2007; 117(1):50–59. [PubMed: 17200706]

48. Vander Heiden MG, Cantley LC, Thompson CB. Understanding the Warburg effect: the metabolic requirements of cell proliferation. Science. 2009; 324(5930):1029–1033. [PubMed: 19460998]

49. Nishiumi S, Shinohara M, Ikeda A, Yoshie T, Hatano N, Kakuyama S, Mizuno S, Sanuki T, Kutsumi H, Fukusaki E. Serum metabolomics as a novel diagnostic approach for pancreatic cancer. Metabolomics. 2010; 6(4):518–528.

50. Olive KP, Jacobetz MA, Davidson CJ, Gopinathan A, McIntyre D, Honess D, Madhu B, Goldgraben MA, Caldwell ME, Allard D, Frese KK, Denicola G, Feig C, Combs C, Winter SP,

Ireland-Zecchini H, Reichelt S, Howat WJ, Chang A, Dhara M, Wang L, Ruckert F, Grutzmann R, Pilarsky C, Izeradjene K, Hingorani SR, Huang P, Davies SE, Plunkett W, Egorin M, Hruban RH, Whitebread N, McGovern K, Adams J, Iacobuzio-Donahue C, Griffiths J, Tuveson DA. Inhibition of Hedgehog signaling enhances delivery of chemotherapy in a mouse model of pancreatic cancer. Science. 2009; 324(5933):1457–1461. [PubMed: 19460966]

51. Provenzano PP, Cuevas C, Chang AE, Goel VK, Von Hoff DD, Hingorani SR. Enzymatic targeting of the stroma ablates physical barriers to treatment of pancreatic ductal adenocarcinoma. Cancer Cell. 2012; 21(3):418–429. [PubMed: 22439937]

52. Kaplan O, Kushnir T, Askenazy N, Knubovets T, Navon G. Role of nuclear magnetic resonance spectroscopy (MRS) in cancer diagnosis and treatment: ^{31}P, ^{23}Na, and ^{1}H MRS studies of three models of pancreatic cancer. Cancer Res. 1997; 57(8):1452–1459. [PubMed: 9108445]

53. Bathen TF, Geurts B, Sitter B, Fjosne HE, Lundgren S, Buydens LM, Gribbestad IS, Postma G, Giskeodegard GF. Feasibility of MR metabolomics for immediate analysis of resection margins during breast cancer surgery. PLoS One. 2013; 8(4):e61578. [PubMed: 23613877]

54. Miccoli P, Torregrossa L, Shintu L, Magalhaes A, Chandran J, Tintaru A, Ugolini C, Minuto MN, Miccoli M, Basolo F, Caldarelli S. Metabolomics approach to thyroid nodules: a high-resolution magic-angle spinning nuclear magnetic resonance-based study. Surgery. 2012; 152(6):1118–1124. [PubMed: 23158182]

55. Yang Y, Wang L, Wang S, Liang S, Chen A, Tang H, Chen L, Deng F. Study of metabonomic profiles of human esophageal carcinoma by use of high-resolution magic-angle spinning ^{1}H NMR spectroscopy and multivariate data analysis. Anal Bioanal Chem. 2013; 405(10):3381–3389. [PubMed: 23455688]

56. Dingley AJ, King NJ, King GF. An NMR investigation of the changes in plasma membrane triglyceride and phospholipid precursors during the activation of T-lymphocytes. Biochemistry. 1992; 31(37):9098–9106. [PubMed: 1390696]

57. Wright LC, Obbink KL, Delikatny EJ, Santangelo RT, Sorrell TC. The origin of ^{1}H NMR-visible triacylglycerol in human neutrophils. High fatty acid environments result in preferential sequestration of palmitic acid into plasma membrane triacylglycerol. Eur J Biochem. 2000; 267(1): 68–78. [PubMed: 10601852]

58. Opstad KS, Bell BA, Griffiths JR, Howe FA. Taurine: a potential marker of apoptosis in gliomas. Br J Cancer. 2009; 100(5):789–794. [PubMed: 19223899]

59. Zhang X, Tu S, Wang Y, Xu B, Wan F. Mechanism of taurine-induced apoptosis in human colon cancer cells. Acta Biochim Biophys Sin. 2014; 46(4):261–272. [PubMed: 24610575]

60. Penet, M-F., Shah, T., Bharti, S., Mironchik, Y., Wildes, F., Maitra, A., Bhujwalla, ZM. Altered choline phospholipid metabolism in pancreatic cancer cells and tumor xenografts. Proceedings of The Joint Annual Meeting ISMRM-ESMRMB; Milan, Italy. 2014; p. 43

61. Glunde K, Bhujwalla ZM, Ronen SM. Choline metabolism in malignant transformation. Nat Rev Cancer. 2011; 11(12):835–848. [PubMed: 22089420]
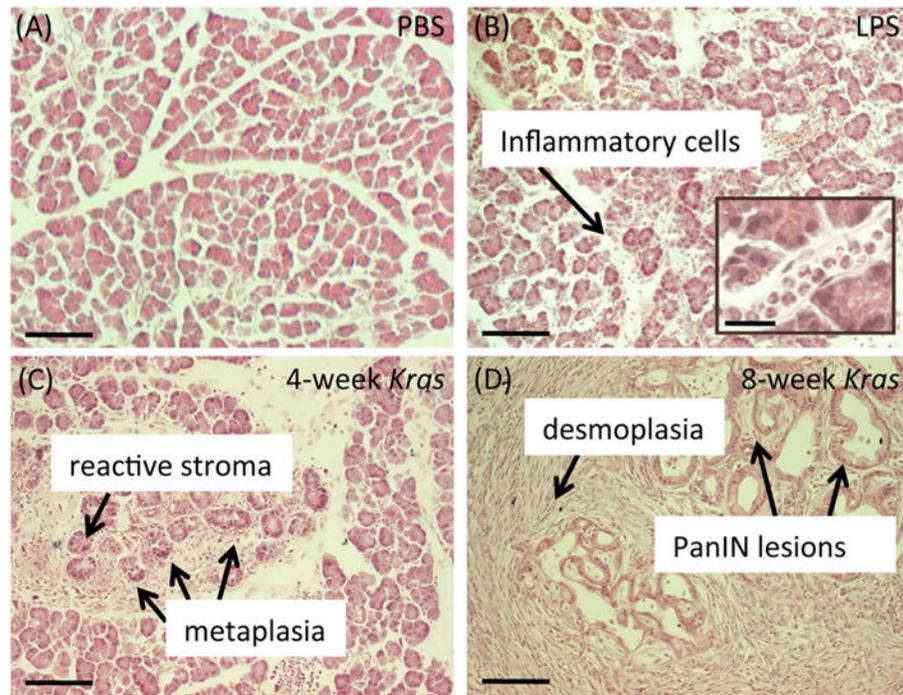
Figure 1.
Histology of LPS-treated and *Kras* mice. (A) Histological section of the pancreas from a wild type mouse treated with PBS. PBS-treated wild type mice display normal tissue architecture devoid of any inflammatory cells or PanIN lesions. (B) Histological section of the pancreas from a wild type mouse treated with LPS. LPS-treated mice contain several inflammatory cells around the normal pancreatic tissue. (C) Histological section of the pancreas from a 4 week old *Kras* mouse. Early stage *Kras* mice display evidence of a reactive stroma, infiltrating inflammatory cells, and acinar to ductal metaplasia. (D) Histological section of the pancreas from an 8 week old *Kras* mouse. These later stage *Kras* mice possess desmoplasia and PanIN lesions. Scale bars, 100 μm. Inset scale bar, 25 μm.
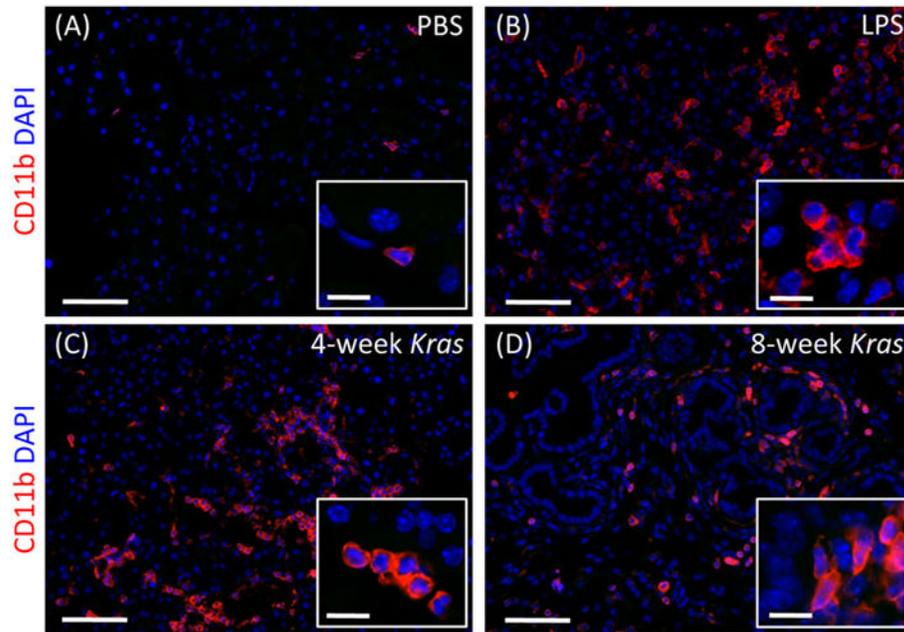
Figure 2.
Levels of inflammation in LPS-treated and *Kras* mice. Pancreatic tissue sections from a PBS-treated wild type mouse (A), LPS-treated wild type mouse (B), 4 week old *Kras* mouse (C), and 8 week old *Kras* mouse (D), DAPI stained (blue) to label the nucleus and CD11b stained (red) to identify in-flammatory cells. (A) PBS-treated wild type mice do not contain any infiltrating cells. (B) LPS-treated mice show extensive infiltration of inflammatory cells in their pancreas. (C) 4 week and (D) 8 week old *Kras* mice both show the presence of inflammatory cells at levels similar to those observed in LPS-treated mice. Scale bars, 50 μm. Inset scale bars, 12 μm.
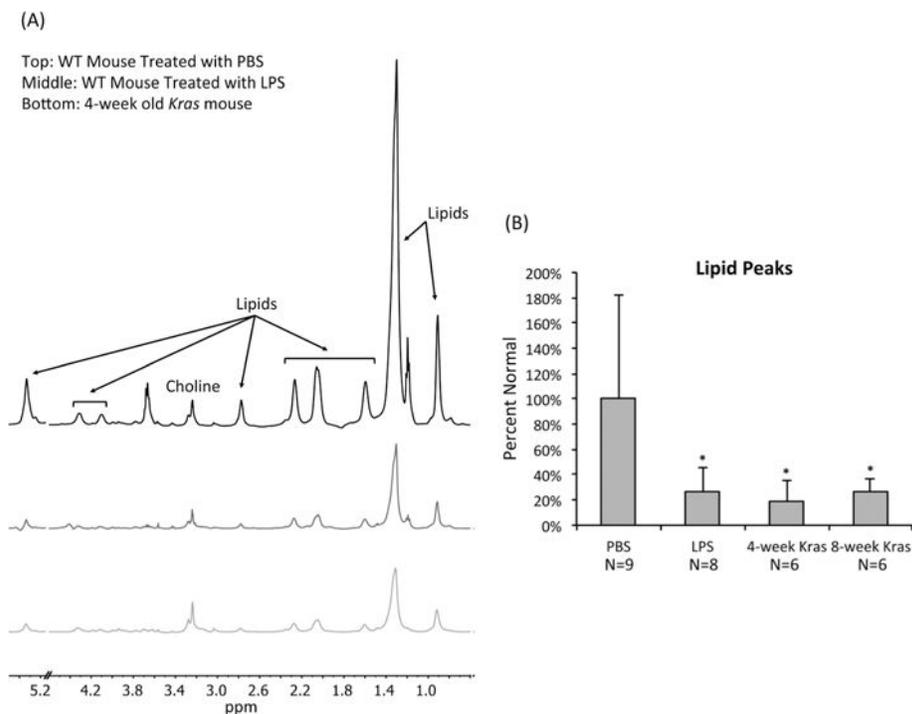
(A)

Top: WT Mouse Treated with PBS
Middle: WT Mouse Treated with LPS
Bottom: 4-week old *Kras* mouse

Figure 3.
Neoplasia is associated with a drop in lipid levels in mouse tissue samples. (A) Representative pulse–acquire spectra of pancreata from a wild type mouse treated with PBS, a wild type mouse treated with LPS, and a 4 week old *Kras* mouse. Spectra display a dramatic drop in lipid levels associated with LPS treatment and *Kras*. All spectra illustrate normalization to sample weight. The peaks at 1.20 and 3.67 ppm are due to the use of ethanol during the tissue collection procedure. The 4.60–5.15 ppm region was removed to exclude the residual water signal. (B) Average levels of lipids present at 1.30 ppm as determined from ^{1}H HR-MAS of pancreatic tissue samples of PBS-treated wild type mice, LPS-treated wild type mice, 4 week old *Kras* mice, and 8 week old *Kras* mice. Lipid levels are lower in LPS-treated wild type, 4 week old *Kras*, and 8 week old *Kras* mice compared with PBS-treated wild type mice. $*p < 0.05$.
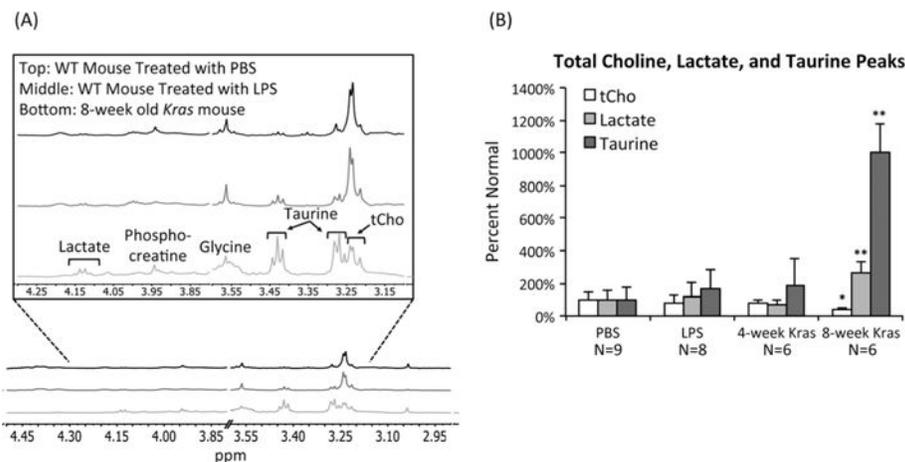
Figure 4.
Neoplasia is associated with high lactate and taurine levels in mouse tissue samples. (A) Representative CPMG spectra of pancreata from a wild type mouse treated with PBS, a wild type mouse treated with LPS, and an 8 week old *Kras* mouse. Spectra display increases in lactate and taurine and a decrease in tCho associated with oncogenic *Kras*. Spectra include peaks for phosphocreatine, glycine, and choline. All spectra illustrate normalization to sample weight. The 3.60–3.80 ppm region was cut to remove the residual ethanol signal resulting from the use of ethanol in collecting tissue samples. (B) Average levels of lactate, taurine, and tCho as determined from ^{1}H HR-MAS of pancreatic tissue samples of PBS-treated wild type mice, LPS-treated wild type mice, 4 week old *Kras* mice, and 8 week old *Kras* mice. Lactate and taurine levels are significantly higher and tCho levels are significantly lower in 8 week old *Kras* mice compared with PBS-treated wild type mice. *$p < 0.05$, **$p < 0.0005$.
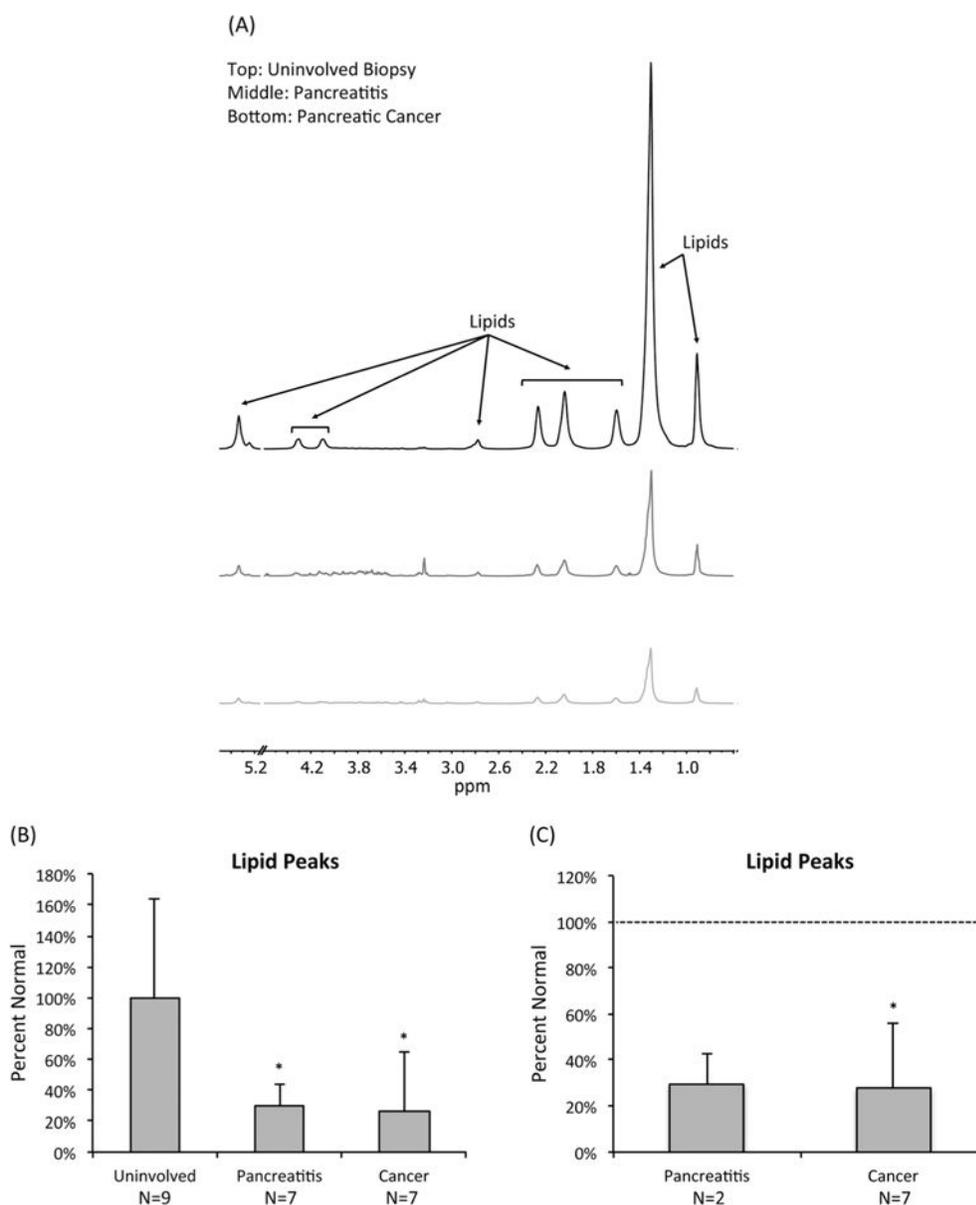
Figure 5.

PDAC is associated with a drop in lipid levels in human tissue samples. (A) Representative pulse–acquire spectra of human pancreata from an uninvolved biopsy, a pancreatitis sample, and a PDAC sample. Spectra display a drop in lipid levels associated with pancreatitis and PDAC. All spectra illustrate normalization to sample weight. The 4.60–5.15 ppm region was removed to exclude the residual water signal. (B) Average levels of lipids at 1.30 ppm as determined from ^{1}H HR-MAS of uninvolved, pancreatitis, and pancreatic cancer tissue samples based on a global analysis without regard to patient matching. Lipid levels dropped significantly in pancreatitis and pancreatic cancer samples. $*p < 0.05$. (C) Average levels of lipids at 1.30 ppm based on a patient-matched analysis. $*p < 0.05$.
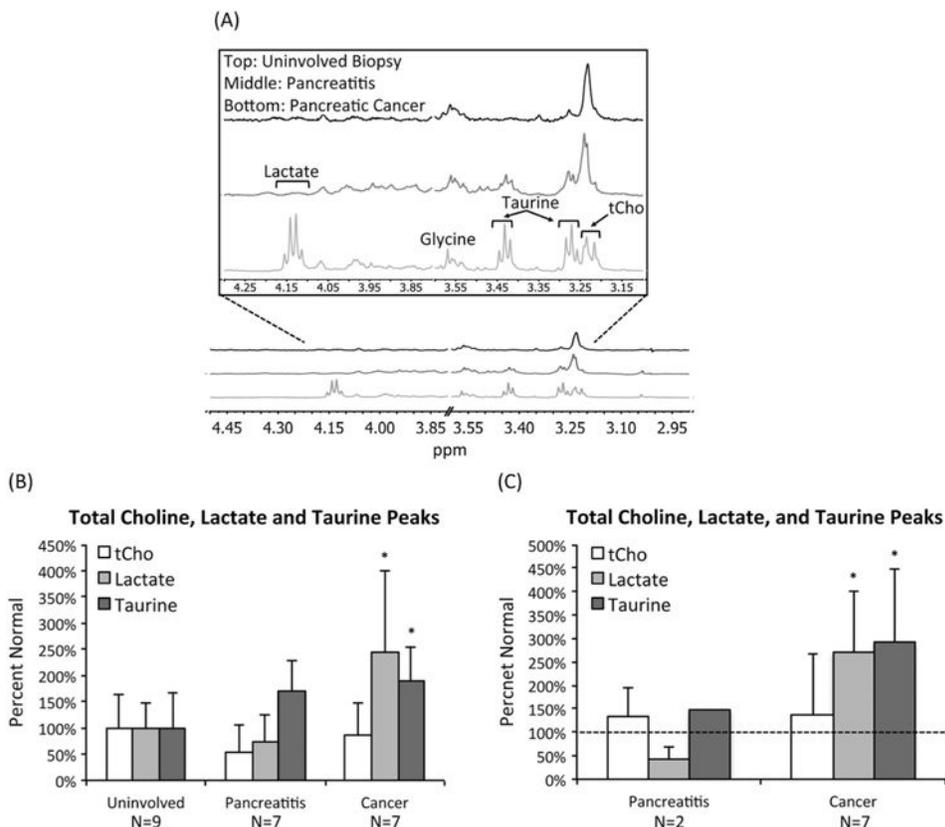
Figure 6.
PDAC is associated with high lactate and taurine levels in human tissue samples. (A) Representative CPMG spectra of human pancreata from an uninvolved biopsy (top), a pancreatitis sample (middle), and a PDAC sample (bottom). Spectra display an increase in lactate and taurine associated with PDAC. All spectra illustrate normalization to sample weight. (B) Average lactate, taurine, and tCho levels as determined from ^{1}H HR-MAS of uninvolved, pancreatitis, and pancreatic cancer tissue samples based on a global analysis without regard to patient matching. Lactate and taurine levels increased significantly in pancreatic cancer samples. *$p < 0.05$. (C) Average lactate, taurine, and tCho levels based on a patient-matched analysis. Both lactate and taurine levels increased significantly in pancreatic cancer samples. *$p < 0.05$.